

# Electrochemical Corrosion Behavior of API X120 Steel at Different Temperatures in CO<sub>2</sub> saturated NaCl solution in presence of 2-[2-(dimethylamino)ethoxy]ethanol as inhibitor

Guo-hua Liang

Guangzhou Institute of Technology, Guangzhou, 510725, China

E-mail: [hellen20000228@163.com](mailto:hellen20000228@163.com), [Guo-huaLIANG@protonmail.com](mailto:Guo-huaLIANG@protonmail.com)

Received: 4 May 2021/ Accepted: 24 June 2021 / Published: 10 August 2021

---

The objectives of this research were to see how the concentration of 2-[2-(dimethylamino)ethoxy] ethanol (DMEE) as an inhibitor, as well as temperature, affected the corrosion rate of API X120 steel in a 3.5wt% NaCl solution saturated with CO<sub>2</sub>. The electrochemical analyses by the potentiodynamic polarization technique showed that the presence of DMEE decreased corrosion current density, and the positive shift of corrosion potential was attributed to the sensible effect of DMEE on the corrosion process due to the creation of a protective layer on the steel surface and it hinders the hydrogen evolution reaction and retards the dissolution reaction. The results demonstrated that DMEE as a mixed inhibitor remarkably decreased the corrosion rate of steel and 87.75% corrosion inhibition efficiency was obtained for the addition of 100µM DMEE in corrosive media at 25°C. Moreover, EIS analyses revealed that the increase in temperature decreased the time lag between the adsorption and desorption of DMEE molecules on the steel surface and led to an increase in corrosion rate and a decrease in inhibition efficiency values with increased temperature. SEM analyses of corroded surface of API X120 steel in presence of DMEE revealed that corrosion was reduced due to the formation of a DMEE protection layer on the metal surface and the capture of CO<sub>2</sub> by DMEE molecules.

---

**Keywords:** Corrosion; Inhibitor; Temperature; 2-[2-(dimethylamino) ethoxy] ethanol; Electrochemical impedance spectroscopy

## 1. INTRODUCTION

Today, industrial development is a major source of air, water and soil pollution. Among these pollutions, air pollution has the potential to significantly degrade the quality of soil and water resources [1]. For example, carbon dioxide (CO<sub>2</sub>), as the most common carbon pollutant can change the ocean's chemistry because of acidification that results from slowing its ability to uptake CO<sub>2</sub> which harms shellfish and marine ecosystems [2, 3]. Moreover, this change increases the corrosion rate of

carbon steel piping and equipment in oil, and consequently enhances the cost of corrosion in oil production and refining. As a result of the fast corrosion rate in the oil and gas production industries, the presence of CO<sub>2</sub> in the deep water environment is a major issue [4].

Many researchers have conducted a study of the effective environmental factors in CO<sub>2</sub> corrosion, such as temperature, pH, concentration of salt, partial pressure, and flow rate [5, 6]. Temperature is the most influential factor in corrosion because the kinetic rate of electrochemical reactions is accelerated by temperature [7].

Furthermore, many studies have been carried out into the type and concentration of corrosion inhibitor as the most suitable method of combating CO<sub>2</sub> corrosion of steel pipelines [8]. The efficiency of inhibitors is attributed to the physicochemical properties and molecular structure which affect the adsorption of the molecules on electrochemical anodic and cathodic sites, and the creation of a protective barrier layer on steel [9, 10]. Furthermore, inhibitor molecules can reduce the rate of reactant diffusion to the metal's surface, and chemical absorption of inhibitor molecules is very effective for CO<sub>2</sub> capture [11].

Therefore, this study was conducted to investigate the effects of 2-[2-(dimethylamino) ethoxy] ethanol (DMEE) concentration as an inhibitor and temperature on the corrosion rate of API X120 steel in a 3.5wt.% NaCl solution saturated by CO<sub>2</sub> gas using electrochemical impedance spectroscopy and potentiodynamic polarization techniques.

## 2. MATERIALS and METHOD

The chemical composition of the API X120 Steel (Hebei Yineng Pipeline Group Co., Ltd, China) was analyzed by an optical emission spectrometer (ICP-OES, iCAP 6000 Duo, Thermo Fisher Scientific, Bremen, Germany). The studied chemical composition is presented in Table 1. The samples were given in 0.5 cm<sup>2</sup> exposed areas. For removal of impurities and oxides from the sample surface, the specimens were polished using 400-grit silicon carbide paper (Global Industrial), rinsed with DI water, and then dried in the air.

The surface morphology of samples was studied by scanning electron microscopy (SEM, JEOL, JSM-6300, Japan).

The electrochemical measurements were performed at various temperatures using a potentiostat/galvanostat system (Gamry, Series 300 /ZRA, Warminster, USA) in an electrochemical cell in a 3.5 wt.% NaCl solution and a CO<sub>2</sub> environment. The pH of the solution was adjusted to 7.2 using 0.1M HCl (37%, Shijiazhuang Xinlongwei Chemical Co., Ltd., China), 0.05M NaOH (99%, Jinan Runqiang Chemical Co., Ltd., China) and a pH meter (Meacon Company, China). The electrochemical cell contained API X120 Steel as the working electrode, a graphite rod as the counter electrode and a saturated calomel electrode (SCE) as the reference electrode. Before all measurements, the samples were immersed in the electrolyte solution at the open-circuit potential (OCP) for 60 minutes to reach the steady state condition. To deactivate the test environment, N<sub>2</sub> gas (99.99%, Qingdao Ruiming Blue Sky Energy Co., Ltd., China) was bubbled into the solution for 100 minutes prior to bubbling CO<sub>2</sub> gas. For reach the CO<sub>2</sub>-saturated solution, 50 cm<sup>3</sup>/min of CO<sub>2</sub> (99.99%, Ningbo

DSW International Co., Ltd., China) was bubbled into the solution for 60 minutes before each measurement and continued during all the electrochemical tests. A thermostat (Julabo F25, Labortechnik GmbH, Germany) was employed to change and adjust the temperature of the solution. The DMEE (98%, Sigma-Aldrich) with different concentrations (20, 50, 80, and 100  $\mu\text{M}$ ) were prepared in deionized water and applied as inhibitors for API X120 Steel corrosion in 3.5wt.% NaCl saturated with  $\text{CO}_2$  gas. Selection of inhibitor concentrations is an important factor in corrosion studies. This concentration range of inhibitor was selected in agreement with the corrosion studies in the literature for DMEE [12] and similar inhibitors such as 2,5-bis(4-dimethylaminophenyl)-1,3,4-oxadiazole [13], 5-(4-Dimethylaminobenzylidene) rhodanine [14], and N-(2-(2-hydroxyethoxy) ethyl)-N, N-dimethylhexadecan-1-ammonium bromide [15]. The electrochemical impedance spectroscopy (EIS) and potentiodynamic polarization (PDP) experiments were carried out in stable OCP conditions. EIS experiments were conducted on AC signal of  $\pm 10\text{mV}$  amplitude and a frequency range from 100 mHz to 100 kHz. The PDP experiments were performed under an applied potential of  $-250\text{ mV}$  to  $+250\text{ mV}$  at a scan rate of  $0.167\text{mV/s}$ .

**Table 1.** API X120 steel chemical compositions

Element	C	Ni	Si	Mn	Cu	Cr	Mo	V	Fe
wt%	0.128	0.016	0.102	0.543	0.016	0.039	0.0013	0.025	Balance

### 3. RESULTS and DISCUSSION

Figure 1 depicts the PDP curves of API X120 steel in a 3.5wt.% NaCl solution saturated by  $\text{CO}_2$  gas and containing different concentrations of DMEE at temperatures of 25, 35, 50, and 85  $^\circ\text{C}$  at a scan rate of  $0.167\text{ mV/s}$ . The corrosion parameters such as corrosion potential ( $E_{\text{corr}}$ ), corrosion current density ( $j_{\text{corr}}$ ), corrosion rate (CR), and corrosion inhibition efficiency (CIE) in Table 2 can be calculated using extrapolating Tafel lines and the following equations [16-19]:

$$\text{CR (mpy)} = \frac{0.13 j_{\text{corr}} A}{nD} \quad (1)$$

$$\theta = \frac{j_{\text{corr}}^0 - j_{\text{corr}}}{j_{\text{corr}}^0} \quad (2)$$

$$\text{CIE} = \theta \times 100 \quad (3)$$

Where A, D and n are the atomic weight, density of iron and the transferred electron number per metal atom, respectively.  $\theta$  is surface coverage, and  $j_{\text{corr}}^0$  and  $j_{\text{corr}}$  are the corrosion current densities of steel in the absence and the presence of the DMEE, respectively. The increase is observed in the current densities of both the anodic and cathodic PDP curves with increasing temperature, and consequently, the corrosion rate of API X120 steel increases which is associated with a higher rate of cathodic hydrogen evolution and anodic metal dissolution [20, 21].

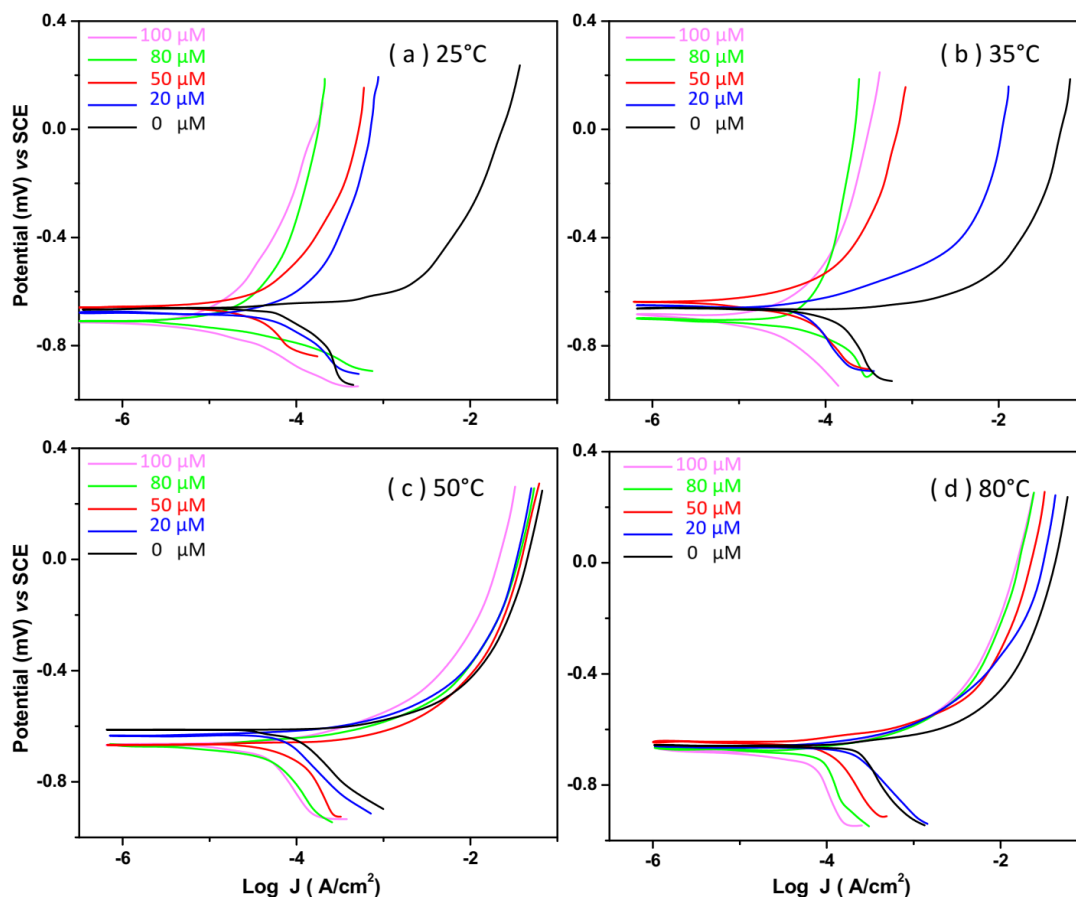


**Figure 1.** PDP curves of API X120 steel into 3.5wt.% NaCl solution saturated by CO<sub>2</sub> gas containing different concentrations of DMEE at temperatures of (a) 25°C, (b) 35°C, (c) 50°C, and (d) 85°C at scan rate of 0.167 mV/s.

Moreover, the presence of DMEE as a corrosion inhibitor changes the corrosion potential and current densities. When the DMEE concentration is increased, both the cathodic and anodic curves are shifted to lower corrosion current values, and the corrosion potential is slightly positive shifted, indicating that DMEE has a perceptible effect on the corrosion process in both anodic and cathodic reactions [22]. Studies have indicated that the inhibitor can be considered as a cathodic or anodic corrosion inhibitor when the displacement in  $E_{\text{corr}}$  is obtained at  $\pm 85$  mV with respect to the  $E_{\text{corr}}$  of the blank (without an inhibitor) [23, 24]. The inhibitor can act as a cathodic corrosion inhibitor when the shift in the  $E_{\text{corr}}$  in the inhibited solution is more than 85 mV, and it can be classified as a mixed inhibitor when the shift is lower than 85 mV [23]. Therefore, it is found in Table 2 that DMEE can act as a mixed inhibitor and reduce CR toward the blank. The lower CR values are observed in high concentrations of DMEE at all temperatures.

**Table 2.** The obtained corrosion parameters from PDP curves for API X120 steels in 3.5wt.% NaCl solution saturated by CO<sub>2</sub> gas containing various concentrations of DMEE at various temperatures at scan rate of 0.167 mV/s.

Temperature (°C)	DMEE concentration (μM)	E <sub>corr</sub> (mV)	j <sub>corr</sub> (μA/cm <sup>2</sup> )	CR (mpy)	CIE (%)
25	0	-698	80	46.45	—
	20	-614	34.2	20.55	57.25
	50	-639	25.1	14.58	68.62
	80	-668	17.9	10.43	77.62
	100	-610	9.8	5.70	87.75
35	0	-659	94.1	54.65	—
	20	-665	46.5	26.99	50.58
	50	-689	40.1	23.28	57.38
	80	-631	30.2	17.54	67.90
	100	-668	17.2	12.21	81.72
50	0	-640	118.2	68.62	—
	20	-697	79.8	37.36	32.48
	50	-677	70.3	34.88	40.52
	80	-639	46.9	27.15	60.32
	100	-673	33.9	19.77	71.31
80	0	-678	181	105.29	—
	20	-640	145.3	84.39	19.72
	50	-649	118.5	68.82	34.53
	80	-620	87.5	50.86	51.65
	100	-640	65.1	37.79	64.03

The reduction in the cathodic and anodic current densities with increasing the DMEE concentration demonstrates DMEE creates a protective layer on the steel surface and hinders the hydrogen evolution reaction and retards the dissolution reaction [10, 26]. Thus, the observations confirm that the presence of the inhibitor can cover part of the steel surface and can block its surface active corrosion sites [10, 27]. Furthermore, there is an increase in CR values with an increase in temperature at the same concentration of the inhibitor. It suggested that the increase in temperature decreases the time lag between the adsorption and desorption of DMEE molecules on the steel surface and consequently, the steel surface experiences longer exposure to the solution, and leads to increase in CR and decrease in CIE values with increasing the temperature [28-30].

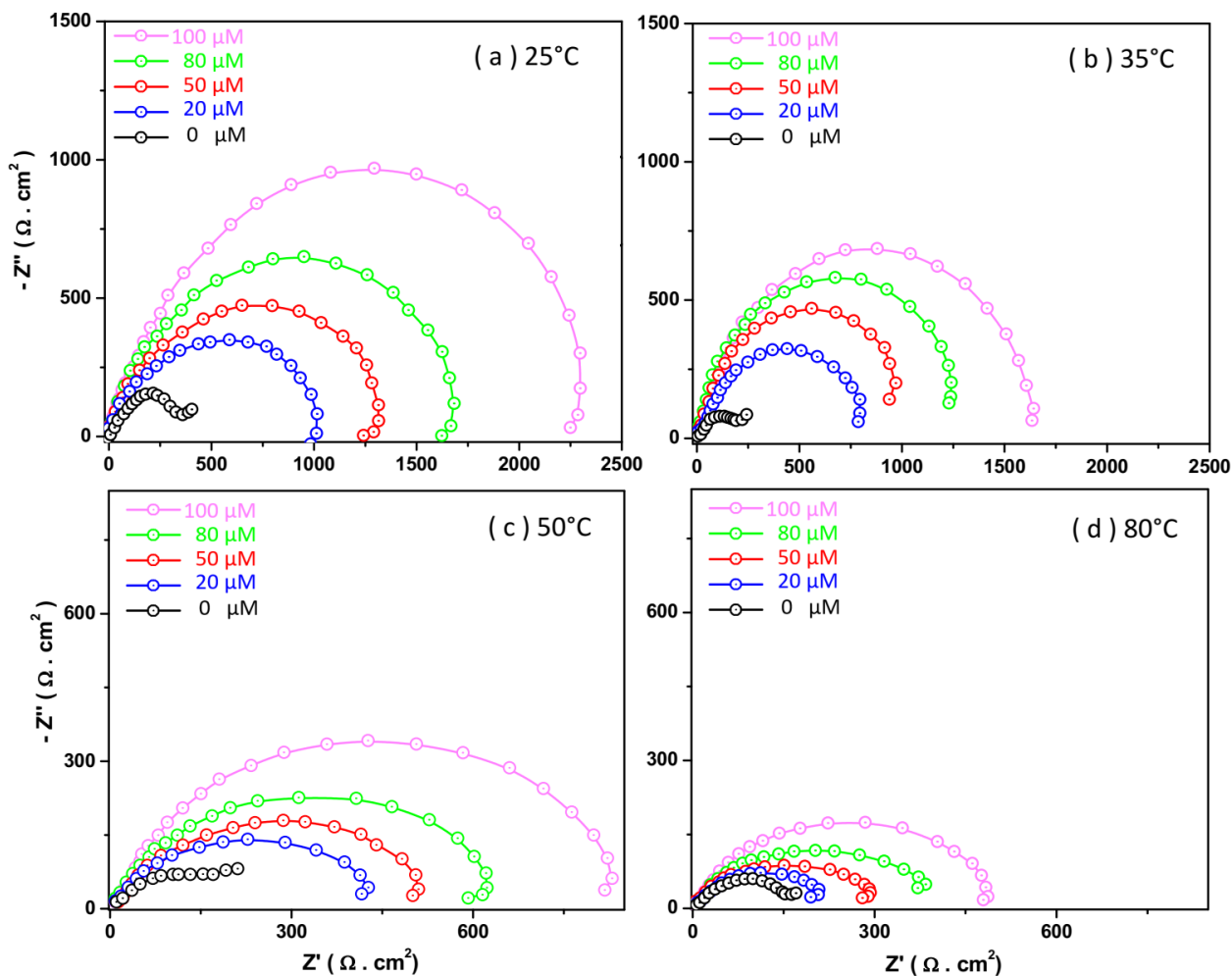


**Figure 2.** EIS measurements of API X120 steel in 3.5wt.% NaCl solution saturated by CO<sub>2</sub> gas with different concentrations of DMEE at temperatures of (a) 25°C, (b) 35°C, (c) 50°C, and (d) 85 °C at scan rate of 0.167 mV/s.

The EIS measurements of API X120 steel in a 3.5wt.% NaCl solution saturated by CO<sub>2</sub> gas with different concentrations of DMEE at various temperatures of 25, 35, 50 and 80 °C at a scan rate of 0.167mV/s are shown in Figure 2. Obviously, the resulting Nyquist plots of EIS display depressed semicircles which refer to the surface heterogeneity of materials [31, 32]. The diameter of the semicircles is increased by increasing the inhibitor concentration, which is attributed to a rise in corrosion resistance [33]. One loop in the Nyquist plots indicated that the charge transfer process is primarily responsible for steel corrosion, and the similar shape in all plots suggests the same corrosion mechanism at all temperatures and inhibitor concentrations [33, 34].

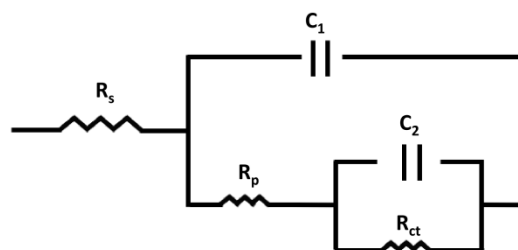


**Figure 3.** The electrical equivalent circuit modeling from EIS data

Furthermore, it is observed that increasing the temperature causes to a decrease in the diameter of the semicircles at the same inhibitor concentration due to the kinetic rate of the electrochemical reactions being accelerated by temperature [29].

Figure 3 exhibits the obtained equivalent electrical circuit which is used as a model to analyze impedance spectra [35]. It includes  $R_s$  and  $R_{ct}$  which indicate solution resistance and charge-transfer resistance, respectively.  $R_p$  is the coating pore resistance that is related to the capacitive loop diameter in the high-frequency region and the corrosion product film on the steel surface [36].  $C_1$  and  $C_2$  represent the capacitance components of the protective corrosion layer and the capacitance of the electric double layer, respectively [36-38]. It describes non-uniform corrosion for an electrode/electrolyte solution interface with two processes in parallel at two time constants that could be ascribed to the roughness or corrosion products on the metal surface [36, 37]. The impedance of the capacitance components ( $Z_Q$ ) can be calculated by equation (4) [16, 17]:

$$Z_Q = \frac{1}{Q_0 (j\omega)^n} \quad (4)$$

Where  $Q_0$  is the capacitance constant,  $n$  is the constant phase number between 0 and 1,  $j$  represents an imaginary number  $((-1)^{1/2})$ , and  $\omega$  shows the angular frequency ( $2\pi f_{\max}$ );  $f_{\max}$  indicates the maximum frequency of the imaginary component. When  $n = 0$ , the capacitance illustrates the pure resistor, and if  $n=1$ , the capacitance displays the pure capacitor [17]. The double layer capacitance ( $C_{dl}$ ) value can be estimated from the following equation [16-19]:

$$C_{dl} = Q_0 \omega^{(n-1)} \quad (5)$$

Moreover, the surface coverage ( $\theta$ ) is also determined according to equation (5) from the analyzing the Nyquist plots [18, 19]:

$$\theta = \frac{R_{ct(\text{inh})} - R_{ct(\text{uninh})}}{R_{ct(\text{inh})}} \quad (6)$$

Where  $R_{ct(\text{inh})}$  and  $R_{ct(\text{uninh})}$  are the charge-transfer resistance values with and without inhibitor, respectively. Table 3 shows all the obtained EIS parameters from analyzing the Nyquist plots. According to the results, the maximum corrosion resistance of API X120 steel is 100  $\mu\text{M}$  of DMEE. A study of the inhibitor concentration and temperature effects reveals that increasing the DMEE concentration increases the  $R_{ct}$  value while increasing the temperature decreases the  $R_{ct}$  value.

Furthermore, the capacitance constant values obtained decreased with increasing DMEE concentration and increased with increasing temperature.

**Table 3.** Electrochemical kinetic parameters obtained from EIS data for API X120 steels in 3.5wt.% NaCl solution saturated by CO<sub>2</sub> gas containing various concentrations of DMEE at various temperatures.

Temperature (°C)	DMEE concentration (μM)	R <sub>s</sub> (Ω.cm <sup>2</sup> )	R <sub>p</sub> (Ω.cm <sup>2</sup> )	R <sub>ct</sub> (Ω.cm <sup>2</sup> )	Q <sub>p</sub> × 10 <sup>-6</sup> (s <sup>n</sup> /Ω.cm <sup>2</sup> )	n <sub>1</sub>	Q <sub>ct</sub> × 10 <sup>-6</sup> (s <sup>n</sup> /Ω.cm <sup>2</sup> )	n <sub>2</sub>	CIE (%)
25	0	12.6	61.9	353.2	155.1	0.89	120.1	0.91	—
	20	12.3	106.2	994	154.3	0.88	70.1	0.98	64.46
	50	11.6	185.1	1402	128.1	0.91	64.1	0.97	74.80
	80	13.8	271.9	1697	127.2	0.89	59.9	0.98	79.18
	100	13.4	140.1	2396	114.2	0.92	50.2	0.88	85.25
35	0	14.3	65.9	297	287.1	0.96	301.2	0.86	—
	20	14.1	20.1	798	229.9	0.75	255.3	0.85	62.78
	50	13.4	29.9	995	224.2	0.84	220.2	0.91	70.15
	80	11.3	35.8	1236	139.9	0.92	168.7	0.96	75.97
	100	12.7	39.7	1691	124.1	0.82	99.8	0.79	82.43
50	0	12.9	19.9	239	299.8	0.77	549.8	0.75	—
	20	10.1	15.1	451	249.9	0.76	385.7	0.86	47.00
	50	11.6	43.7	561	225.6	0.97	324.1	0.97	57.39
	80	12.1	19.9	683	166.2	0.93	289.5	0.91	65.00
	100	10.9	30.1	869	138.2	0.71	290.2	0.79	72.49
80	0	11.3	24.1	173	319.8	0.59	861.1	0.85	—
	20	12.5	35.2	235	301.1	0.71	624.2	0.98	26.38
	50	12.6	45.9	298	250.2	0.89	569.8	0.61	41.94
	80	13.8	49.9	403	223.8	0.78	567.3	0.94	57.07
	100	12.4	56.2	493	221.9	0.61	529.4	0.95	64.90

According to the Helmholtz equation (7), these observations can be explained by an inverse proportion relationship between double layer capacitance and the thickness of the adsorbed layer of corrosion inhibitor on the API X120 steel ( $\delta_{ads}$ ) [9, 39, 40]:

$$\delta_{\text{ads}} = \frac{\epsilon\epsilon_0 A}{C_{\text{dl}}} = \frac{\epsilon\epsilon_0 A}{Q_0 \omega^{(n-1)}} \quad (7)$$

Where  $A$  is electrode surface area exposed to the corrosive medium,  $\epsilon_0$  is permittivity of air, and  $\epsilon$  is local dielectric constant. Accordingly, the equation exhibits that capacitance constant and double layer capacitance is inversely proportional to the thickness of the adsorbed inhibitor on steel surface which confirms that the decline of the double layer capacitance can be ascribed to the enhancement of the adsorbed layer of DMEE with increasing the DMEE concentration in solution [39, 41]. Thus, the enhancement of the adsorbed layer of DMEE on steel as a protective film slows down the electron transfer rate [39, 42]. The decrease in CIE with increasing temperature might be associated with desorption of the DMEE molecules from the metal surface at higher temperatures [39, 42]. In consequence, PDP measurements are in good agreement with those obtained EIS results.

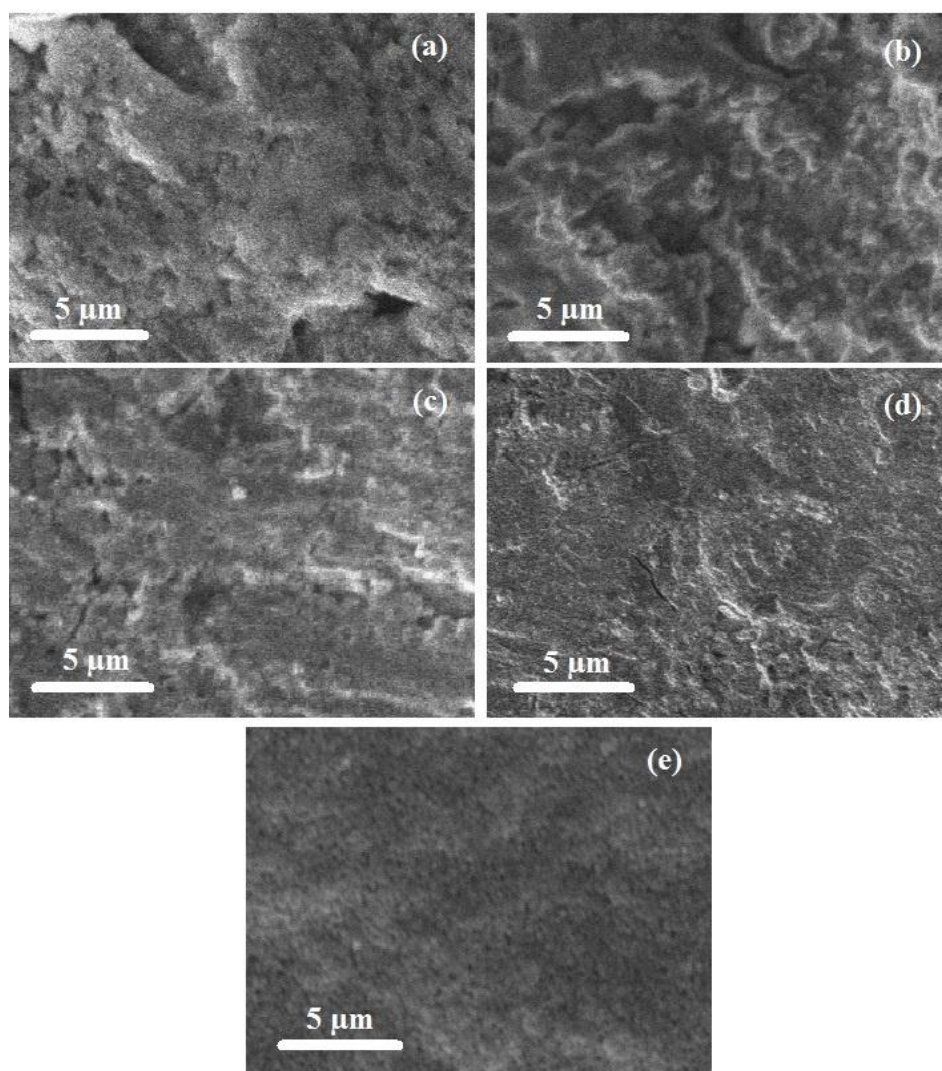


**Figure 4.** SEM images for API X120 steels (a) before immersion, and after 7 hours immersion in corrosive medium at temperatures of 25°C containing (b) 3.5 wt.% NaCl solution, (c) 3.5 wt.% NaCl solution with 100 μM of DMEE, (d) 3.5wt.% NaCl solution saturated by CO<sub>2</sub> gas, and (e) 3.5wt.% NaCl solution saturated by CO<sub>2</sub> gas with 100 μM of DMEE.

Further study was conducted on the surface morphology of steel after exposure in corrosive medium after 7 hours of immersion in 3.5 wt.% NaCl solution with and without 100  $\mu\text{M}$  of DMEE at temperatures of 25°C. Figure 4a indicates SEM image of surface of API X120 steel before of exposure in NaCl solution. Figure 4b displays the SEM image of corroded surface of API X120 steels into 3.5wt.% NaCl with pitting corrosion and rough rust layer due to attack of chloride ions toward the passive layer. Figure 4c depicts the morphology of API X120 steel surface in 3.5wt.% NaCl solution with 100  $\mu\text{M}$  of DMEE, indicating to formation of limited amount of localized deep pits due to aggregation of corrosion products at the pit mouths [43]. Figure 4d shows SEM image of studied steel in 3.5wt.% NaCl solution saturated by CO<sub>2</sub> gas, representing the formation of dense porous corrosion scale because of formation of carbonic acid by dissolution of CO<sub>2</sub> gas in aquatic media [44, 45]. Figure 4e shows SEM image of studied steel in 3.5 wt.% NaCl solution saturated with CO<sub>2</sub> gas in presence of 100  $\mu\text{M}$  of DMEE, revealing the decrease of corrosion due to formation of protection layer of DMEE on metal surface and capturing the CO<sub>2</sub> by DMEE molecules [46].

#### 4. CONCLUSION

This study was conducted on investigating the effects of DMEE concentration as inhibitor and temperature on the corrosion rate of API X120 steel in 3.5wt.% NaCl solution saturated by CO<sub>2</sub> gas by EIS and PDP techniques. Results showed that presence of DMEE caused to shift to lower corrosion current density, and the corrosion potential was slightly positive shifted which related to perceptible effect of DMEE on corrosion process in both anodic and cathodic reactions due to creation a protective layer on the steel surface and hinders hydrogen evolution reaction and retards the dissolution reaction. The results indicated that DMEE as a mixed inhibitor remarkably decreased corrosion rate of steel and 87.75% corrosion inhibition efficiency was obtained for addition of 100 $\mu\text{M}$  DMEE in corrosive solution at 25°C. Furthermore, electrochemical studies showed that the increase in temperature decreased the time lag between the adsorption and desorption of DMEE molecules on the steel surface and led to increase in corrosion rate and decrease in inhibition efficiency values with increasing the temperature. SEM analyses the corroded surface of X120 steels into 3.5wt.% NaCl solution in presence of DMEE exhibited the decrease of corrosion because of formation of protection layer of DMEE on metal surface and capturing the CO<sub>2</sub> by DMEE molecules.

#### References

1. M. Sun, L. Yan, L. Zhang, L. Song, J. Guo and H. Zhang, *Process Biochemistry*, 78 (2019) 108.
2. J. Hartmann, A.J. West, P. Renforth, P. Köhler, C.L. De La Rocha, D.A. Wolf-Gladrow, H.H. Dürr and J. Scheffran, *Reviews of Geophysics*, 51 (2013) 113.
3. H. Zhang, W. Guan, L. Zhang, X. Guan and S. Wang, *ACS omega*, 5 (2020) 18007.
4. Z. Yang, P. Xu, W. Wei, G. Gao, N. Zhou and G. Wu, *IEEE Transactions on Plasma Science*, 48 (2020) 2822.
5. G. Cui, Z. Yang, J. Liu and Z. Li, *International Journal of Greenhouse Gas Control*, 90 (2019) 102814.
6. Y. Li, D.D. Macdonald, J. Yang, J. Qiu and S. Wang, *Corrosion Science*, 163 (2020) 108280.
7. H.-S. Oh, J.-H. Lee and H. Kim, *International journal of hydrogen energy*, 37 (2012) 10844.

8. Y. Liu, T. Xu, Y. Liu, Y. Gao and C. Di, *Journal of Materials Research and Technology*, 9 (2020) 8283.
9. F. El-Hajjaji, R. Belkhemima, B. Zerga, M. Sfaira, M. Taleb, M.E. Touhami, B. Hammouti, S. Al-Deyab and E. Ebenso, *International Journal of Electrochemical Science*, 9 (2014) 4721.
10. M. Abdallah, M. Hegazy, M. Alfakeer and H. Ahmed, *Green Chemistry Letters and Reviews*, 11 (2018) 457.
11. N. Kladkaew, R. Idem, P. Tontiwachwuthikul and C. Saiwan, *Energy Procedia*, 4 (2011) 1761.
12. A. Fouda, S. Rashwan, S.M. Shaban, H.E. Ibrahim and M. Elbhrawy, *Egyptian journal of petroleum*, 27 (2018) 295.
13. M. Bouanis, M. Tourabi, A. Nyassi, A. Zarrouk, C. Jama and F. Bentiss, *Applied Surface Science*, 389 (2016) 952.
14. R. Solmaz, *Corrosion Science*, 79 (2014) 169.
15. S.M. Shaban, A. Fouda, S. Rashwan, H.E. Ibrahim and M. Elbhrawy, *Protection of Metals and Physical Chemistry of Surfaces*, 54 (2018) 709.
16. A.S.K. Zadeh, M. Shahidi-Zandi and M. Kazemipour, *International Journal of Electrochemical Science*, 15 (2020) 10802.
17. M.M. Solomon, H. Gerengi, T. Kaya, E. Kaya and S.A. Umoren, *Cellulose*, 24 (2017) 931.
18. D.B. Hmamou, A. Zarrouk, R. Salghi, H. Zarrok, E.E. Ebenso, B. Hammouti, M. Kabanda, N. Benchat and O. Benali, *International Journal of Electrochemical Science*, 9 (2014) 120.
19. A. Zarrouk, H. Zarrok, R. Salghi, N. Bouroumane, B. Hammouti, S. Al-Deyab and R. Touzani, *International Journal of Electrochemical Science*, 7 (2012) 10215.
20. R. Liu, M. Hurley, A. Kvrryan, G. Williams, J. Scully and N. Birbilis, *Scientific reports*, 6 (2016) 1.
21. Q. Wang, S. Sun, X. Zhang, H. Liu, B. Sun and S. Guo, *Bioresource Technology*, 332 (2021) 125120.
22. M. Al-Otaibi, A. Al-Mayouf, M. Khan, A. Mousa, S. Al-Mazroa and H. Alkathlan, *Arabian Journal of Chemistry*, 7 (2014) 340.
23. J.A. Rodríguez, J. Cruz-Borbolla, P.A. Arizpe-Carreón and E. Gutiérrez, *Materials*, 13 (2020) 5656.
24. J.-B. Liu, M. Ren, X. Lai and G. Qiu, *Chemical Communications*, 57 (2021) 4259.
25. M. Zhang, *International Journal of Electrochemical Science*, 16 (2021) 1.
26. G. Palumbo, M. Górny and J. Banaś, *Journal of Materials Engineering and Performance*, 28 (2019) 6458.
27. M.P. Chakravarthy, K.N. Mohana and C.B. Pradeep Kumar, *International Journal of Industrial Chemistry*, 5 (2014) 19.
28. X. Xu, A. Singh, Z. Sun, K. Ansari and Y. Lin, *Royal Society open science*, 4 (2017) 170933.
29. C. DeWaard and D. Williams, *Industrial finishing and surface coatings* 28 (1976) 24.
30. Y. Duan, Y. Liu, Z. Chen, D. Liu, E. Yu, X. Zhang, H. Fu, J. Fu, J. Zhang and H. Du, *Green Chemistry*, 22 (2020) 44.
31. N. Mahato and M. Singh, *Portugaliae Electrochimica Acta*, 29 (2011) 233.
32. Z. Chen, H. Zhang, X. He, G. Fan, X. Li, Z. He, G. Wang and L. Zhang, *BioResources*, 16 (2021) 2644.
33. E. Ituen, O. Akaranta and A. James, *Journal of King Saud University-Engineering Sciences*, 31 (2019) 191.
34. M. Manssouri, Y. El Ouadi, M. Znini, J. Costa, A. Bouyanzer, J. Desjobert and L. Majidi, *Journal of Materials and Environmental Science*, 6 (2015) 631.
35. S.M. Abdulrahim, Z. Ahmad, J. Bahadra and N.J. Al-Thani, *Nanomaterials*, 10 (2020) 1635.
36. S. Feliu, *Metals*, 10 (2020) 775.
37. A. Singh, M. Talha, X. Xu, Z. Sun and Y. Lin, *ACS omega*, 2 (2017) 8177.

38. L. Zhang, M. Zhang, S. You, D. Ma, J. Zhao and Z. Chen, *Science of The Total Environment*, 780 (2021) 146505.
39. A. Sehmi, H. Ouici, A. Guendouzi, M. Ferhat, O. Benali and F. Boudjellal, *Journal of the Electrochemical Society*, 167 (2020) 155508.
40. L. Zhang, J. Zheng, S. Tian, H. Zhang, X. Guan, S. Zhu, X. Zhang, Y. Bai, P. Xu and J. Zhang, *Journal of Environmental Sciences*, 91 (2020) 212.
41. M. Zhang, L. Zhang, S. Tian, X. Zhang, J. Guo, X. Guan and P. Xu, *Chemosphere*, 253 (2020) 126638.
42. E.B. Caldona, M. Zhang, G. Liang, T.K. Hollis, C.E. Webster, D.W. Smith Jr and D.O. Wipf, *Journal of Electroanalytical Chemistry*, 880 (2021) 114858.
43. J. Tang, J. Li, H. Wang, Y. Wang and G. Chen, *Applied Sciences*, 9 (2019) 706.
44. H. Bai, Y. Wang, Y. Ma, Q. Zhang and N. Zhang, *Materials*, 11 (2018) 1765.
45. F. Guo, S. Wu, J. Liu, Z. Wu, S. Fu and S. Ding, *Engineering Fracture Mechanics*, 248 (2021) 107711.
46. G. Fytianos, S.J. Vevelstad and H.K. Knuutila, *International Journal of Greenhouse Gas Control*, 50 (2016) 240.

© 2021 The Authors. Published by ESG ([www.electrochemsci.org](http://www.electrochemsci.org)). This article is an open access article distributed under the terms and conditions of the Creative Commons Attribution license (<http://creativecommons.org/licenses/by/4.0/>).